Cancer Research

Transfer of miRNA in Macrophage-Derived Exosomes Induces Drug Resistance in Pancreatic Adenocarcinoma

Yoav Binenbaum[1], Eran Fridman[1], Zvi Yaari[2], Neta Milman[1], Avi Schroeder[2], Gil Ben David[1], Tomer Shlomi[3], and Ziv Gil[1,4]

Abstract

Pancreatic ductal adenocarcinoma (PDAC) is known for its resistance to gemcitabine, which acts to inhibit cell growth by termination of DNA replication. Tumor-associated macrophages (TAM) were recently shown to contribute to gemcitabine resistance; however, the exact mechanism of this process is still unclear. Using a genetic mouse model of PDAC and electron microscopy analysis, we show that TAM communicate with the tumor microenvironment via secretion of approximately 90 nm vesicles, which are selectively internalized by cancer cells. Transfection of artificial dsDNA (*barcode fragment*) to murine peritoneal macrophages and injection to mice bearing PDAC tumors revealed a 4-log higher concentration of the *barcode fragment* in primary tumors and in liver metastasis than in normal tissue. These macrophage-derived exosomes (MDE) significantly decreased the sensitivity of PDAC cells to gemcitabine, *in vitro* and *in vivo*. This effect was mediated by the transfer of miR-365 in MDE. miR-365 impaired activation of gemcitabine by upregulation of the triphospho-nucleotide pool in cancer cells and the induction of the enzyme cytidine deaminase; the latter inactivates gemcitabine. Adoptive transfer of miR-365 in TAM induced gemcitabine resistance in PDAC-bearing mice, whereas immune transfer of the miR-365 antagonist recovered the sensitivity to gemcitabine. Mice deficient of *Rab27 a/b* genes, which lack exosomal secretion, responded significantly better to gemcitabine than did wildtype. These results identify MDE as key regulators of gemcitabine resistance in PDAC and demonstrate that blocking miR-365 can potentiate gemcitabine response.

Significance: Harnessing macrophage-derived exosomes as conveyers of antagomiRs augments the effect of chemotherapy against cancer, opening new therapeutic options against malignancies where resistance to nucleotide analogs remains an obstacle to overcome. *Cancer Res; 78(18); 5287–99.* ©*2018 AACR.*

Introduction

Pancreatic ductal adenocarcinoma (PDAC) ranks fourth among cancer-related deaths. Despite decades of research, the cure rate of the disease remains disappointingly low (<5%; ref. 1). This dismal prognosis is due to late detection and to resistance of tumors to all known systemic therapies.

Gemcitabine, the first-line drug for the treatment of PDAC, is a cytidine analog that acts to inhibit cell growth by arrest of DNA replication. Resistance to gemcitabine develops within weeks of initiation of therapy, as a result of intrinsic resistance and environmental factors (2). Gemcitabine is metabolized intracellularly by deoxycytidine kinase (dCK), to active phospho-nucleosides; the incorporation of these nucleosides into DNA and RNA leads to replication arrest. Among the mechanisms known to cause gemcitabine resistance are loss of membranal transporters, deficiency of dCK, competition with *de novo* CTP, and upregulation of cytidine deaminase (CDA), the enzyme that metabolizes gemcitabine to its inactive form. Treatment with nab-paclitaxel was shown to reduce CDA expression and potentiate gemcitabine efficacy; this highlights the importance of CDA in mediating drug resistance (3).

Macrophages are associated with poor prognosis in PDAC (4) and were shown to secrete soluble factors that induce gemcitabine resistance of PDAC cells (5). We hypothesized that tumor-associated macrophages (TAM) secrete vesicles that transfer molecular signals to cancer cells, thus inducing drug resistance.

Here, we demonstrate a mechanism by which resistance to chemotherapy is mediated through shuttling of miRNAs between TAM and cancer cells, via exosomes.

Materials and Methods

Animals

All animal experiments were approved by The Institutional Animal Care and Use Committee at the Technion, approval# IL-086-07-2013 and IL-124-12-2012. Wild-type (WT) C57/bl

[1]The Laboratory for Applied Cancer Research, Department of Otolaryngology Head and Neck Surgery, Clinical Research Institute at Rambam Healthcare Campus, Haifa, Israel. [2]Laboratory for Targeted Drug Delivery and Personalized Medicine Technologies, Technion, Israel Institute of Technology, Haifa, Israel. [3]Departments of Computer Science and Biology, Technion, Israel Institute of Technology, Haifa, Israel. [4]Technion Integrated Cancer Center, Rappaport Institute of Medicine and Research, Technion, Israel Institute of Technology, Haifa, Israel.

Note: Supplementary data for this article are available at Cancer Research Online (http://cancerres.aacrjournals.org/).

Corresponding Author: Ziv Gil, Rambam Medical Center, Haifa 3525408, Israel. Phone: 972-4-7772480; E-mail: G_Ziv@rambam.health.gov.il

doi: 10.1158/0008-5472.CAN-18-0124

mice were purchased from Harlan. *Rab27a*$^{-/-}$*b*$^{-/-}$ were a kind gift from Miguel C. Seabra of the National Heart and Lung Institute, Imperial College, London, United Kingdom. *Rab27a*$^{-/-}$*b*$^{-/-}$ mice were bred and genotyped as described (6, 7).

Tissue culture

PDAC K989 cell line is an in-house line, generated from an explant culture of a pancreatic tumor from a KPC mouse (8). Cells were authenticated by sequencing of *Kras G12D* and *TP53 R172H* mutations, and *pdx-1* CRE insertion (primers are detailed in Supplementary Table S1). The following early passage ATCC cell lines were used in our experiments: NIH-3T3 (ATCC CRL-1658 passage 8–12), Mia PaCa 2 (ATCC CRL-1420 passage 3–7), and THP-1 (ATCC TIB-202, passage 3–6). All cells were tested for *Mycoplasma* on a regular basis. Murine peritoneal macrophages (mpMacrophages) were isolated from the peritoneal lavage of WT C57/Bl mice or *Rab27a*$^{-/-}$*b*$^{-/-}$ mice. mpMacrophages were incubated for 24 hours with 100 ngr/mL LPS and 20 ngr/mL γ-IFN for M1 polarization, and with 20 ngr/ml IL4 (Peprotech) for M2 polarization. Polarization was verified by RT-PCR for the transcripts Arginase-1, CD206, CD86, and iNOS, as described (9). THP-1 monocytes were differentiated to macrophages as described (10), except that 100 ng/mL of phorbol 12-myristate 13-acetate (Sigma; P8139) was used. Macrophages were polarized toward the M2 phenotype as described above, using human IL4 (Peprotech).

Exosome purification and characterization

Exosomes were isolated from macrophage conditioned media as described previously (11). One dose corresponded to exosomes from 30 mL media. Unless otherwise stated, one dose of exosomes was used. Exosome size distribution and concentrations were assessed with the Nanoparticle Tracking Analysis (NTA) system (Nanosight NS300). One dose contained approximately 2 μg of protein, and 5×10^{11} exosomes, as measured by Nanosight. RNA was extracted by the Hybrid-R miRNA purification Kit (GeneAll). Cryo-TEM sample preparation and acquisition, and NTA sample acquisition and analysis are described in the Supplementary Data Section.

Exosome internalization experiments

Exosomes were labeled with PKH67 (Sigma) or CFSE (Molecular Probes) according to the manufacturer's instructions. Excess dye was removed using exosome spin columns (Thermo Fisher Scientific). PKH67-stained exosomes were applied on cells for 75 minutes, and cells were then vigorously washed thrice. Cells were fixed by 4% PFA and counterstained by PKH26 (Sigma). Slides were viewed on a LSM-550 confocal microscope (Ziess), with a X63 objective, through a pinhole of 120 to 134 μm, with 23–30 Z-stacks per field of view. Images were analyzed using Imaris software with an Imaris-Cell module (Bitplane) that identified the nucleus and the cell membrane.

Gene expression RT-qPCR, Western blot analysis, and immunofluorescence were previously described (12–15). Western blotting and immunoprecipitation are described in Supplementary Materials. Supplementary Tables S2 and S3 provide lists of antibodies and qPCR primers used in the study. For miRNA detection, RT-qPCR was performed with commercial TaqMan MicroRNA Assays (ABI, Thermo Fisher Scientific) using 5 ngr of small RNA per reaction. U6 was used as an internal control. For these experiments, primers designed for the homo sapiens miRNAs were used, due to complete sequence homology. Assay IDs are detailed in Supplementary Table S4.

More methods are described in the Supplementary Methods section in the Supplementary Materials.

Results

Secretion of exosomes from mpMacrophages

The accumulation of TAM (bearing M2 markers) in sections from patients with PDAC, together with our previous findings that M2-polarized macrophages are involved in gemcitabine resistance, led us to investigate the mechanism of M2 macrophage–induced drug resistance (5). M2-polarized murine mpMacrophages were generated by adding cytokine IL4 to the media (Supplementary Fig. S1A; refs. 9, 16). The media were purified by differential centrifugations (11) and examined by a cryogenic transmission electron microscope. The electron microscope imaging revealed the presence of nanovesicles of variant sizes (Fig. 1A; Supplementary Fig. S1B; ref. 17). The diameter distribution of these nanovesicles revealed a mean size of 90 nm for cryopreserved spheres (Fig. 1B), or a mean diameter of 135 nm in room temperature (Supplementary Fig. S1C). This variation in size can be explained by expansion of vesicle volume at room temperature, relative to the cryo-TEM environment (17, 18), or by inherent differences between measurement techniques (electron microscope vs. NTA; ref. 19). Immunoblotting of lysates from purified nanovesicles, using known exosomal markers (11, 20, 21), demonstrated that these nanovesicles expressed CD63 and LAMP2 (Fig. 1C). This observation, together with the size distribution, suggested that these were MDE.

MDE and gemcitabine resistance

As M2 mpMacrophages can secrete soluble signals that induce chemotherapy resistance, we conjectured that MDE may also play a role in this process. We evaluated the effect of gemcitabine on PDAC K989 cells in the presence of MDE. MDE significantly decreased the sensitivity of K989 cells to gemcitabine (Fig. 1D, $P < 0.01$ at 5–50 μmol/L of gemcitabine). At a gemcitabine concentration of 50 μmol/L, the survival of K989 cells was increased by 100% after adding MDE compared with control ($P = 0.001$). MDE affected the response of K989 cells to gemcitabine (5 μmol/L) in a dose-dependent manner ($P = 0.02$, Fig. 1E). Similar to the KPC cell line, the MiaPaCa-2 human pancreatic cell line incubated with MDEs from THP-1 cells also demonstrated reduction of sensitivity to gemcitabine (Fig. 1F, $P < 0.05$).

Selectivity of MDE

To further investigate the mode of interaction between MDE and cancer cells, MDE were stained by the lipophilic dye, PKH67 (green), and incubated with nonfixed K989 cells for 75 minutes, followed by vigorous washing. After fixation, the cell membranes were stained with PKH26 (red). MDE could be detected in the cytoplasm of cancer cells (Fig. 2A). Analysis of the intracellular architecture revealed that cytoplasmic spheres culminated close to the plasma membrane (Fig. 2B and C; Supplementary Fig. S1D). These data suggest that exosomes secreted by M2 mpMacrophages are readily internalized by K989 cells.

Next, we evaluated the selectivity of MDE, by comparing their uptake by cancer cells and stromal cell monocultures. We first incubated K989 cells and fibroblasts (NIH-3T3) in the presence of PKH67-labeled MDE for 75 minutes and evaluated the MDE

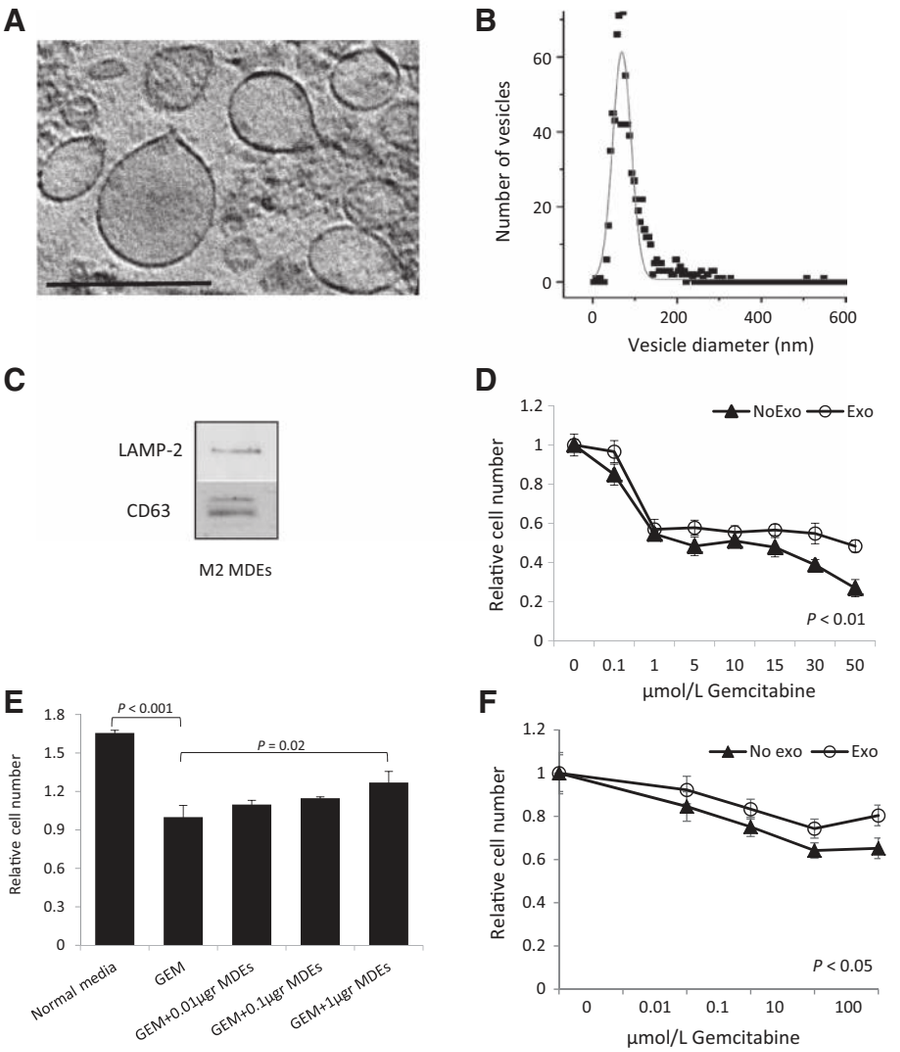

Figure 1.
MDE and gemcitabine resistance. **A,** Cryo-TEM image of exosomes in mouse peritoneal macrophage media (bar, 200 nm). **B,** Distribution of exosome diameters measured in the cryo-TEM images. **C,** Western blot analysis of exosomes from M2-polarized mpMacrophages. **D,** Proliferation of K989 cells, pretreated with exosomes (empty circles) or control (filled triangles), incubated with escalating doses of gemcitabine ($P < 0.001$). Samples were normalized to proliferation without gemcitabine. **E,** Proliferation of K989 cells treated with escalating doses of MDE ±5 µmol/L gemcitabine ($P = 0.02$). Samples were normalized to proliferation without gemcitabine. **F,** Proliferation of MiaPaCa-2 cells, pretreated with THP-1–derived exosomes (empty circles bars) or control (filled triangles), incubated with escalating doses of gemcitabine ($P < 0.001$). Samples were normalized to proliferation with gemcitabine only.

uptake levels by measuring the green PKH67 signal in each cell line. Supplementary Fig. S2A shows that 26.6% of the K989 cells were positive for PKH67, whereas none of the fibroblasts showed positive MDE uptake ($P < 0.001$, Supplementary Fig. S2A). Despite the detection of a robust exosome signal in the cytoplasm of K989 cells, immunofluorescence microscopy detected only low signal levels in NIH-3T3 cells (Supplementary Fig. S2B). To further evaluate exosomal distribution in PDAC tumors *ex vivo*, tumors from 5-month-old KPC mice were dissociated to a single-cell suspension and plated to adhere to a tissue culture dish. The cells were incubated with PKH67-labeled MDE and analyzed by flow cytometry. Supplementary Fig. S2C demonstrates that anti–cytokeratin antibody-stained K989 cells, but not NIH-3T3 fibroblast or mpMacrophages. In 21.5% of the CK^+ cancer cells, intracellular PKH67-labeled exosomal staining was observed, compared with 0.38% of the CK-negative cells (Fig. 2D; Supplementary Fig. S2D).

To investigate whether macrophages transfer exosomes to pancreatic cancer cells *in vivo*, we synthesized a unique 75-nt-long dsDNA "*barcode fragment,*" which was transfected to mpMacrophages. Following verification of the barcode in MDE (Supplementary Fig. S2E), barcode-transfected mpMacrophages were injected i.p. to mice carrying K989-PDAC tumors. Mice were sacrificed after 48 hours, and their organs were separately dissociated to single-cell suspensions. Tumor cells (CK-positive) and mpMacrophages (F4/80 positive) were sorted by FACS, and the abundance of the barcode in these populations was assessed by qRT-PCR. Figure 2E shows that in both the primary tumors and the liver metastases, the DNA *barcode* accumulated predominantly in CK^+ PDAC cells compared with the CK-negative stromal cells ($P < 0.001$). Uptake in the normal pancreas, spleen, and liver was 4–5 log less than in the primary tumor or in metastases. Overall, these results suggest a selective transfer of exosomes from mpMacrophages to cancer cells, both *ex vivo* and *in vivo*.

Exosomal transfer of miRNA from macrophages to PDAC cells

Growing evidence indicates that exosomes are enriched in miRNAs (22, 23). Analysis of the content of MDE using the Agilent Bioanalyzer RNA LabChip revealed abundant short RNAs measuring 18–22 nt, the size of miRNAs (Supplementary Fig. S3A), whereas RNA fragments longer than 200 nt were not evident in MDE (Supplementary Fig. S3B). A literature search revealed

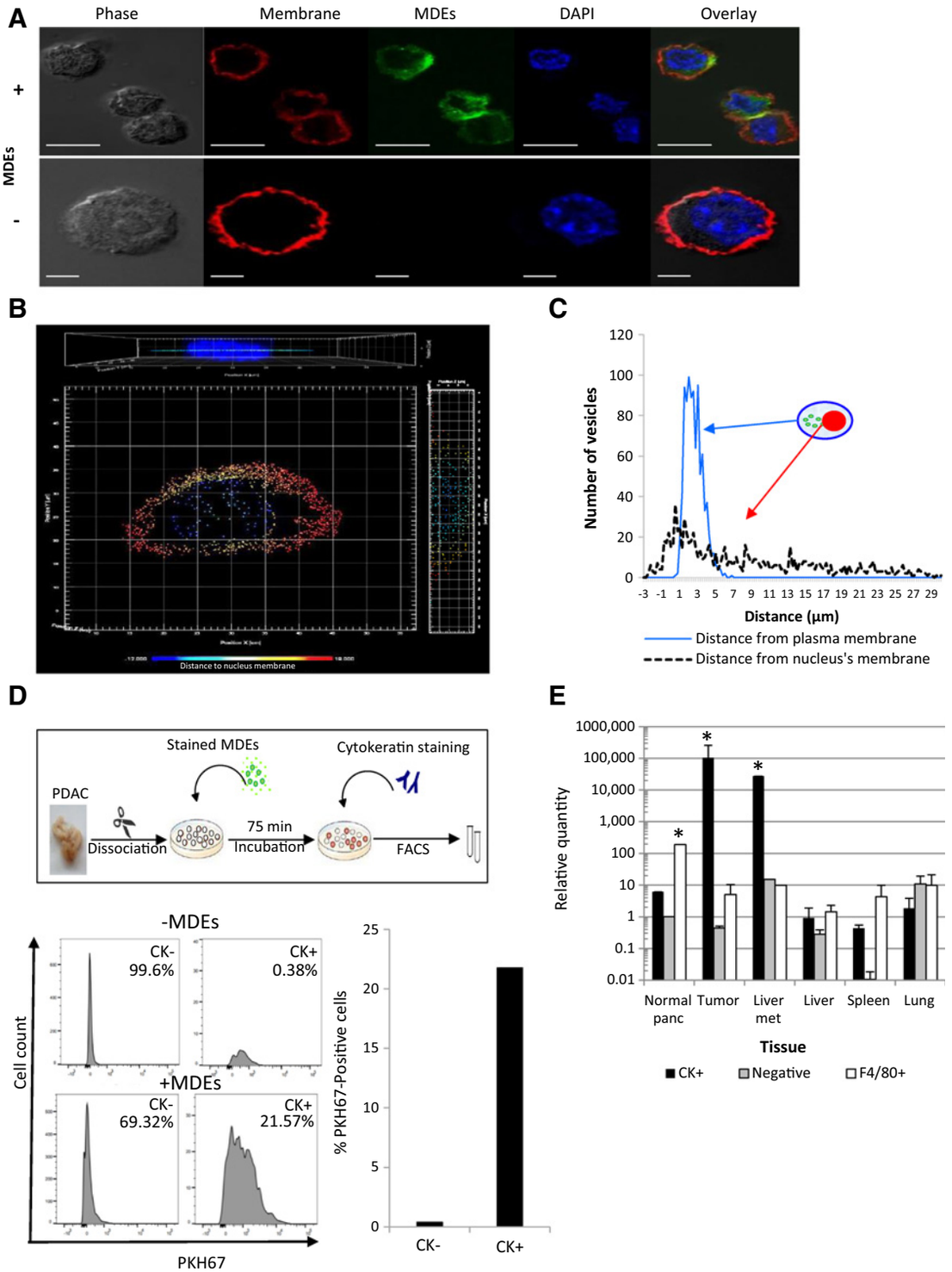

Figure 2.

Selectivity of MDE. **A,** Confocal images of K989 cells with or without stained exosomes (green). Cell membranes are shown in red (bar, 10 μm). **B,** 3D cell image of exosome distribution inside a K989 cell. **C,** Analysis of the distance of internalized exosomes from the plasma membrane or nucleus. Negative values denote exosomes inside the nucleus. **D,** Exosome internalization by K989 cells. Top, experiment design. Bottom, FACS analysis of exosome (PKH67) uptake by K989 cells (cytokeratin-positive) or stromal cells (cytokeratin-negative). The bar graph shows percentages of PKH67-positive in indicated cell populations. **E,** qPCR for detection of the ds-DNA *barcode*, recovered from indicated tissue: PDAC cells (CK^+), macrophages ($F4/80^+$), and stromal cells (negative). *, $P < 0.001$. panc, pancreas; met, metastasis.

that miRNAs 21,181b, 320, 365, and Let-7a were previously implicated in the induction of chemotherapy resistance (24–26, 27). We profiled the miRNA content of M1 and M2 mpMacrophages using nCounter Mouse miRNA Expression Assay (Nanostring). We found miR-365 to rank among the most differentially upregulated miRNAs in M2 compared with M1 mpMacrophages (Supplementary Table S5). The relative abundance of miRNAs 21,181b, 320, 365, and Let-7a was compared by real-time PCR in M1 and M2 mpMacrophage MDE. Figure 3A shows that MDE from M2 mpMacrophages were rich in miRNAs 181b, 320, and 365, relative to exosomes from M1 (3.82-, 3.39-, and 10.25-fold, respectively; $P = 0.04$, $P = 0.01$, and $P = 0.002$, respectively). miRNAs 320, 181b, and 21, but not miR-365 and Let-7a, were also enriched in exosomes secreted from M2 macrophages compared with exosomes secreted from naïve (M0) macrophages (Supplementary Fig. S3C). Incubation of K989 cells with gemcitabine further induced miR-181b and miR-365 expression (Fig. 3B). Most importantly, incubation of K989 cell MDE and gemcitabine had a profound *synergistic* effect on miR-365 expression compared with other miRNAs. The finding that miR-365 is markedly upregulated in K989 cells treated with gemcitabine and MDE suggests its potential role in gemcitabine resistance.

Exosomal transfer of miR-365 induces gemcitabine resistance

We next investigated the role of miR-365 transfer by MDE in gemcitabine resistance. To this end, we performed a series of miR-365 perturbations in K989 cells and evaluated the contribution of M2 mpMacrophages to gemcitabine resistance. Transfection of miR-365 mimic to K989 cells significantly increased the miR-365 levels compared with controls ($P = 0.01$), whereas antagomiR-365 transfection significantly reduced miR-365 expression in the cancer cells ($P = 0.03$). Incubation with MDE increased the expression of miR-365 in K989 cells, whereas transfection of antagomiR-365 to K989 cells significantly reduced the effect of MDE on miR-365 levels (Fig. 3C, $P < 0.01$). We incubated K989 cells with MDE alone, or transfected K989 cells with 50 nmol/L or 100 nmol/L of antagomiR-365, and then incubated them with MDE. Comparing the amounts of miR-365 in these cells, we found that antagomiR transfection reduced the increase observed by incubation with MDE in a dose-dependent manner (Supplementary Fig. S3D). Congruent with these results, Fig. 3D shows that transfection of miR-365 to K989 cells induced gemcitabine resistance relative to miR-control, whereas transfection of antagomiR-365 to K989 cells restored the effect of gemcitabine ($P = 0.01$). Previous studies have demonstrated that overexpression of miR-365 can inhibit proliferation (28). K989 cells treated with M2 MDE or miR-365 without gemcitabine showed increased proliferation levels, indicating that gemcitabine resistance did not result from reduced proliferation (Supplementary Fig. S3E).

To further assess the effect of miR-365 transfer by exosomes, we cocultured K989 cells and M2 mpMacrophages in a transwell system. AntagomiR-365 transfection to M2 mpMacrophages resulted in a dramatic reduction in miR-365 expression in mpMacrophages (Supplementary Fig. S3F). mpMacrophages transfected with antagomiR-365 or miR-control were plated in inserts with 220-nm pore size and incubated with K989 cells for 48 hours (Fig. 3E). K989 cells were then harvested and analyzed by qRT-PCR and FACS for miR-365 expression and apoptosis. Figure 3F shows that K989 cells incubated with mpMacrophages transfected with miR-control had significantly higher miR-365 levels than cells incubated with M2 mpMacrophages transfected with antagomiR-365 ($P = 0.01$).

Figure 3G shows that M2 mpMacrophages transfected with miR-control induced a significantly lower level of cell death and apoptosis (30.1% and 20.23%, respectively) in K989 cells than did M2 mpMacrophages transfected with antagomiR-365 when incubated with gemcitabine (73.2% and 55.5%, respectively). Taken together, these data show that exosomal transfer of miR-365 via exosomes induced gemcitabine resistance, and that antagomiR-365 treatment of the mpMacrophages can restore the sensitivity of cancer cells to gemcitabine.

Exosomal modulation of pyrimidine metabolism and CDA expression in PDAC

To further explore the mechanism by which MDE and miR-365 induce gemcitabine resistance, we analyzed, by liquid chromatography–mass spectrometry (LC/MS), cell lysates of K989 cells incubated with MDE or transfected with miR-365 mimic. Heat maps of the top 50 metabolites of K989 cells treated with MDE and miR-365 mimic are presented in Fig. 4A and B and Supplementary Table S6, respectively. The analysis revealed a significant increase in pyrimidine metabolism of K989 by MDE or miR-365 (Fig. 4C and D, respectively, $P < 0.001$), and a significant increase in triphosphate-nucleotide (NTP) concentration in both miR-365–transfected and MDE-treated K989 cells compared with controls (Fig. 4E and F). Metabolomic analysis of M2-derived exosomes did not detect high levels of nucleotides that could account for the observed increase in nucleotide pools in K989 cells after treatment with MDE or miR-365 (Supplementary Metabolomics Data MDE).

High levels of NTPs upregulate CDA, the enzyme that controls the cellular pyrimidine pool, by catalyzing cytidine to uridine (29). CDA inactivates gemcitabine by converting dFdCytidine to dFdUridine (2). Figure 4G shows that increasing intracellular NTPs upregulates CDA expression in K989 cells. To examine the possibility that miR-365 and MDE upregulate CDA expression, we transfected miR-365 mimic to K989 cells and evaluated CDA expression by four methods. A qRT-PCR analysis demonstrated that transfection of miR-365 mimic increased *CDA* transcript levels in a dose-response manner ($P < 0.05$), whereas antagomiR-365 significantly reduced the relative expression of *CDA* ($P = 0.04$; Fig. 4H). The expression of the gemcitabine transporter *hENT1* did not change significantly after treatment of K989 cells with MDE or transfection with miR-365 mimic compared with controls (MDE+/MDE–, RQ = 1.9, $P > 0.05$; miR-control/miR-365, RQ = 0.9, $P > 0.1$). Similarly, increased CDA protein levels were observed when K989 cells were incubated with MDE or transfected with miR-365 mimic (Fig. 4I). LC/MS analysis of K989 cells, incubated for 48 hours with MDE, had a 2.6-fold higher concentration of dFdUridine in their media than did controls ($P = 0.01$, Fig. 4J). This supports the hypothesis that increased CDA expression is a component of the mechanism by which MDE and miR-365 reduce sensitivity to gemcitabine. In agreement, LC/MS analysis revealed a significant increase in dFdUridine in the media of K989 cells transfected with miR-365 mimic compared with miR-control, 16 hours after initiation of the experiment (Fig. 4K, $P = 0.02$). Immune precipitation did not reveal the presence of CDA protein in MDE, ruling out the possibility that direct CDA transport occurs via exosomes (Fig. 4L).

The above results show that MDE and miR-365 modulate pyrimidine metabolism in PDAC cells. Increasing NTP

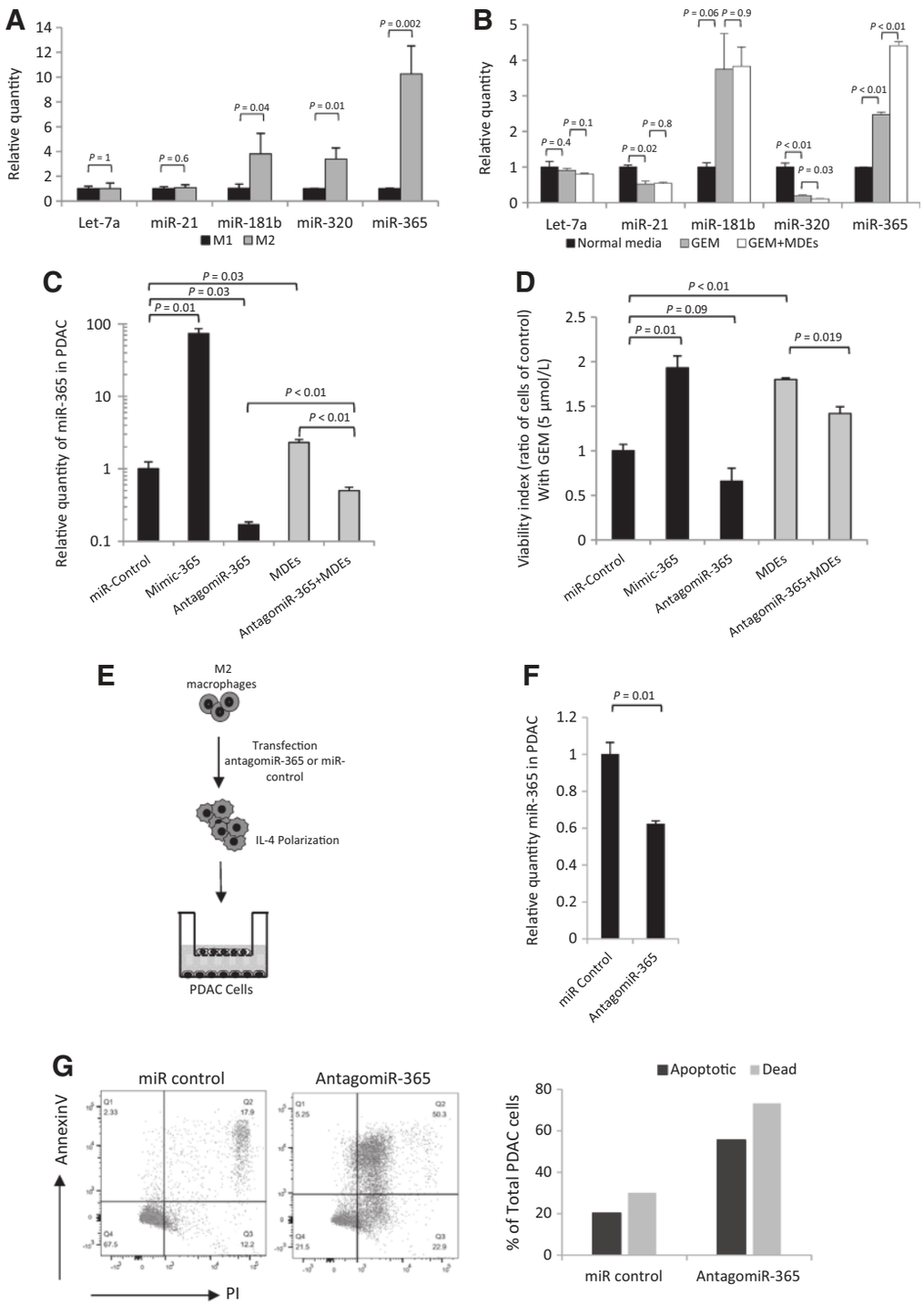

Figure 3.

Exosomal transfer of miR-365 induces gemcitabine resistance. **A,** Relative enrichment of indicated miRNAs in M1- and M2-derived exosomes, measured by qRT-PCR. miRNA levels in M1 NDEs were used for normalization. **B,** Modulation of miRNA abundance in K989 cells by gemcitabine (GEM), gemcitabine with exosomes (GEM+MDE), and control (normal media), as evaluated by qRT-PCR. miRNA levels in K989 cells grown in control media were used for normalization. **C,** miR-365 perturbation in K989 cells. Black bars, K989 cells transfected with miR-control, miR-365 mimic, or antagomiR-365. Gray bars, K989 cells treated with MDEs with or without antagomiR-365 transfection in the presence of 5 μmol/L gemcitabine. miRNA levels in cells transfected with miR-control were used for normalization. **D,** The effect of perturbations described in **C** on K989 cell proliferation in the presence of gemcitabine (5 μmol/L). Proliferation of K989 cells transfected with miR-control was used for normalization. **E,** Experimental design. K989 cells cocultured with M2 mpMacrophages transfected with miR-control or antagomiR-365. **F,** miR-365 expression in K989 cells. miR-365 levels in K989 cells cocultured with mpMacrophages transfected with miR-control were used for normalization. **G,** FACS analysis of K989 cells cocultured with M2 mpMacrophages transfected with antagomiR-365/miR-control (gemcitabine 5 μmol/L). Bar graph, Apoptosis and cell death levels in K989 cells from M2 mpMacrophages+antagomiR-365 and miR-M2 mpMacrophages+miR-control groups.

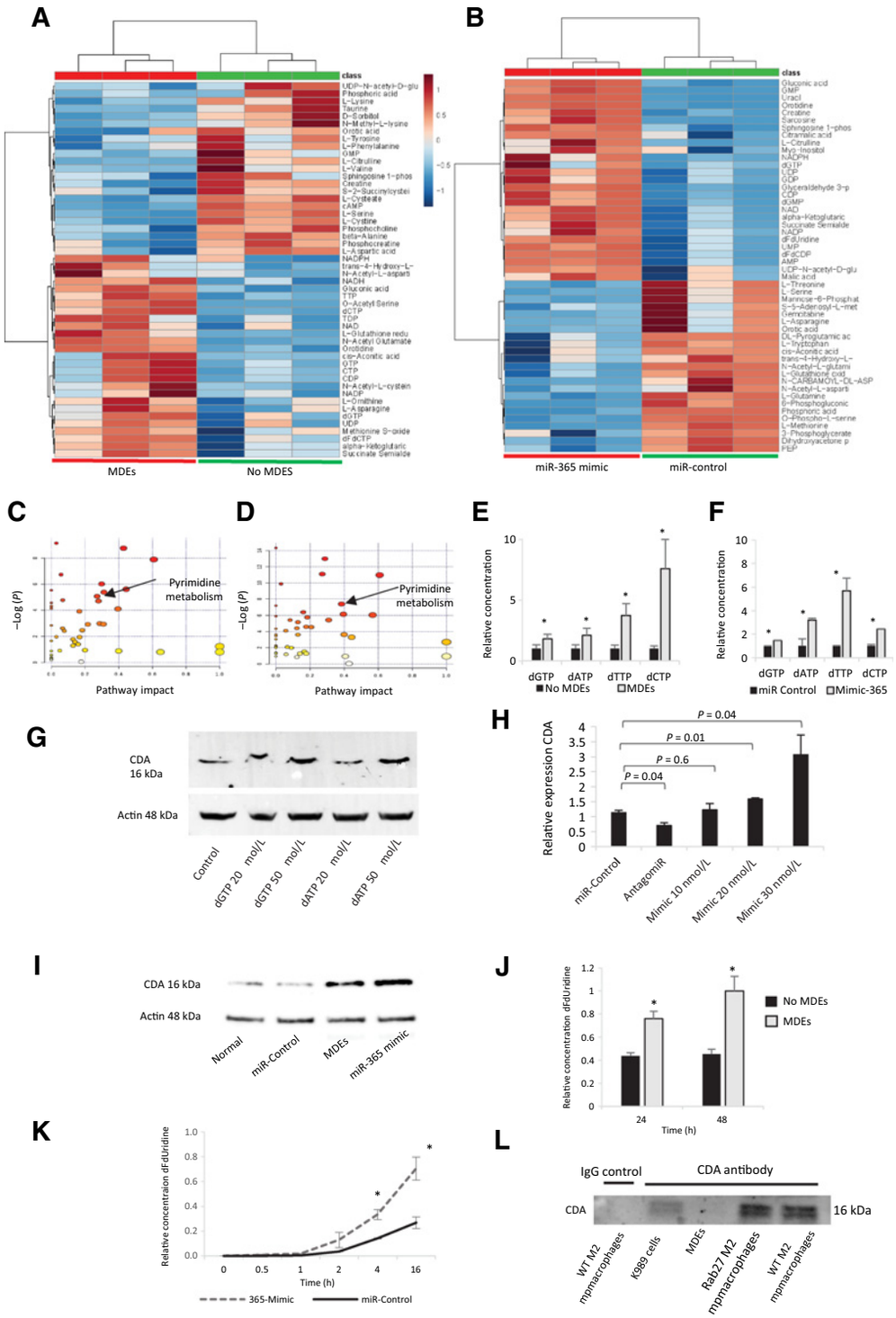

Figure 4.

Macrophage-derived exosomes and miR-365 regulate pyrimidine synthesis and CDA expression. **A,** Heat map of LC-MS metabolomics. Abundant metabolites for K989 cells pretreated with MDE or control and incubated with gemcitabine (5 μmol/L). **B,** Heat map of LC-MS metabolomics of K989 cells transfected with miR-365 or miR-control and incubated as in **A**. **C, "**Metabolome view" for pathway enrichment cells treated as in **A**. **D,** Concentration of dNTPs, measured by LC/MS analysis in K989 cells, with or without MDE (*, $P < 0.05$). **E, "**Metabolome view" for pathway enrichment cells treated as in **B**. **F,** Concentration of dNTPs, measured by LC/MS analysis in K989 cells, transfected with miR-365 or miR-control (*, $P < 0.05$). **G,** Western blot of CDA in K989 cells loaded with increased concentrations of NTPs (dGTP/dATP). **H,** qPCR of CDA expression in K989 cells transfected with indicated oligonucleotides (gemcitabine 5 μmol/L). CDA levels in K989 cells transfected with miR-control were used for normalization. **I,** Western blot of CDA in K989 cells treated as indicated. **J,** LC/MS analysis of dFdUridine excreted by K989 cells, with/without MDE (*, $P = 0.01$). **K,** MS analysis of dFdUridine excreted by K989 cells treated as indicated (*, $P = 0.02$). **L,** Immunoprecipitation of CDA from lysates prepared from K989 cells and MDE as indicated.

concentration induced miR-365–upregulated CDA expression. CDA inactivates gemcitabine by its conversion to dFdUridine (2). Increased concentration of NTPs in PDAC cells also promoted gemcitabine resistance, as dCTP competes with dFdCTP for DNA incorporation.

Modulation of gemcitabine resistance *in vivo*

To investigate the contribution of MDE to gemcitabine resistance *in vivo*, we used the *Rab27a*$^{-/-}$*b*$^{-/-}$ (Rab27KO) mouse model. Rab27KO mice have impaired exosomal packaging and secretion due to hampered intracellular trafficking (7, 30). Rab27KO mpMacrophages had significantly lower exosome secretion than did WT controls ($P = 0.05$, Supplementary Fig. S4A and S4B; ref. 24).

We implanted the pancreata of WT and Rab27KO mice with PDAC K989 cells and followed tumor size by small animal sonography ($n = 8$ per group). The tumor kinetics were similar between Rab27KO and WT mice 7 weeks after tumor implantation (Supplementary Fig. S4C, $P = 0.49$).

At 2 weeks after implantation, the mean tumor volume was similar in both groups. Next, both groups were treated with gemcitabine for 5 weeks (Fig. 5A). Figure 5B shows the tumor growth kinetics in each animal separately. As shown in Fig. 5C, 5 weeks after gemcitabine treatment, tumors in the Rab27KO group responded significantly better to chemotherapy than did those in the WT group (274 ± 223 mm^3 and 865 ± 545 mm^3, respectively, $P = 0.003$). Immunofluorescence analysis of sections from the animal described above, stained with anti-F4/80 and anti-CDA (Fig. 5D and E), demonstrated that although the distribution of mpMacrophages was similar in both groups (105 vs. 122; F4/80+ cells/field, $P = 0.51$, Fig. 5F), CDA expression in PDAC tumors was significantly lower in Rab27KO mice than in WTs (mean fluorescence intensity of 2.6 and 9.1, respectively, $P < 0.05$, Fig. 5G). CDA staining intensity was similar in 5-week postimplantation tumors induced in WT and Rab27KO without gemcitabine treatment (Supplementary Fig. S4D). Supplementary Fig. S4E demonstrates CDA expression in cytokeratin-positive ductal cells in the tumor. Cytokeratin-positive cells had more intense CDA staining than cytokeratin-negative cells in WT and Rab27KO tumors (Supplementary Fig. S4E and S4F).

Immune transfer of antagomiR-365 augments gemcitabine response

To overcome the effect of miR-365 on gemcitabine resistance, we used mpMacrophages as carriers of antagomiR-365. We implanted K989 PDAC tumors in Rab27KO mice to minimize endogenous MDE secretion. This enabled manipulation of exosomes predominantly in the immune-transferred mpMacrophages. Tumors were grown in the pancreata of Rab27KO mice for 2 weeks. We then performed immune transfer of mpMacrophages to the PDAC-bearing Rab27KO mice (5 million mpMacrophages/dose, i.p. injection, twice weekly), with three distinct macrophage populations: WT donor mpMacrophages transfected with antagomiR-365 ($n = 6$), WT donor mpMacrophages transfected with miR-control ($n = 7$), and mpMacrophages from Rab27KO donors transfected with miR-control ($n = 6$). Mice were then treated with gemcitabine and followed for 10 weeks (Fig. 6A). Immunofluorescence of pancreatic specimens demonstrated similar macrophage density in tumors from all groups (T TEST WT+miR-control, Rab27KO+miR-control, $P = 0.6$; T TEST WT+miR-control, WT+antagomiR-365, $P = 0.2$). Our staining cannot distinguish between endogenous and immune-transferred mpMacrophages (Fig. 6B). CDA expression was significantly higher in the group treated with WT mpMacrophages transfected with miR-control than in those treated with Rab27KO mpMacrophages transfected with miR-control, or with WT mpMacrophages transfected with antagomiR-365 ($n = 6$–7 mice, $P < 0.05$, Fig. 6B and C). Kaplan–Meier graphs showed that mice injected with WT mpMacrophages transfected with miR-control had significantly shorter survival than mice treated with WT mpMacrophages transfected with antagomiR-365 ($P = 0.03$, Fig. 6D). Similarly, mice injected with WT mpMacrophages transfected with miR-control had shorter survival than mice injected with Rab27KO mpMacrophages transfected with miR-control ($P = 0.01$). Mice injected with WT mpMacrophages transfected with miR-control had larger tumors than mice treated with WT mpMacrophages transfected with antagomiR-365, and than mice injected with Rab27KO mpMacrophages transfected with miR-control (Supplementary Fig. S4G). Overall, the data show that immune transfer of antagomiR-365 via mpMacrophages can restore sensitivity to gemcitabine *in vivo*.

Discussion

In this work, we uncovered a mechanism by which macrophages communicate with PDAC cells to induce chemotherapy resistance. We showed that miRNAs containing MDE are transferred from macrophages to PDAC cells, altering their gene expression and metabolism. The latter results in excretion of gemcitabine out of cells and chemotherapy resistance.

Accumulating evidence suggests that the tumor microenvironment plays a pivotal role in the development of drug resistance (2, 31). M2 macrophages are a prominent constituent in the pancreatic cancer microenvironment and have been associated with poor prognosis (32, 33), neural invasion (4, 34), and poor response to treatment (35). However, the mechanism for intercellular communication between macrophages and PDAC cells is poorly understood. Here, we demonstrated that macrophages transmit molecular signals to cancer cells by shuttling exosomes that are selectively internalized by PDAC cells. We found most of the internalized MDE to be cytosolic and close to the plasma membrane; and a minority of the signals was perinuclear. Exosomes appear to selectively enter cancer cells *ex vivo*, but rarely to enter their noncancerous stromal counterparts.

In vivo, the dsDNA barcode that was delivered from TAM- to PDAC-bearing mice was recovered almost exclusively from cancer cells in primary tumors and in distant metastases. Selective uptake of exosomes by cancer cells can be explained by protein–protein interactions, by specific lipid properties, or by macropinocytosis.

Both receptor-mediated endocytosis, requiring the recognition of a specific ligand by a receptor on the host cell, and raft-mediated endocytosis, requiring the presence of cholesterol and sphingolipid-rich microdomains, were implicated in exosome internalization (28). Ras-transformed PDAC cells were reported to display enhanced micropinocytosis (36). This could explain the preferential uptake of exosomes by PDAC cells compared with other stromal cells.

MDE-mediated transfer of miR-365 plays a pivotal role in chemotherapy resistance, as MDE-treated K989 cells display increased survival in response to gemcitabine, relative to untreated controls. We found that in the transfer of miR-365, MDE

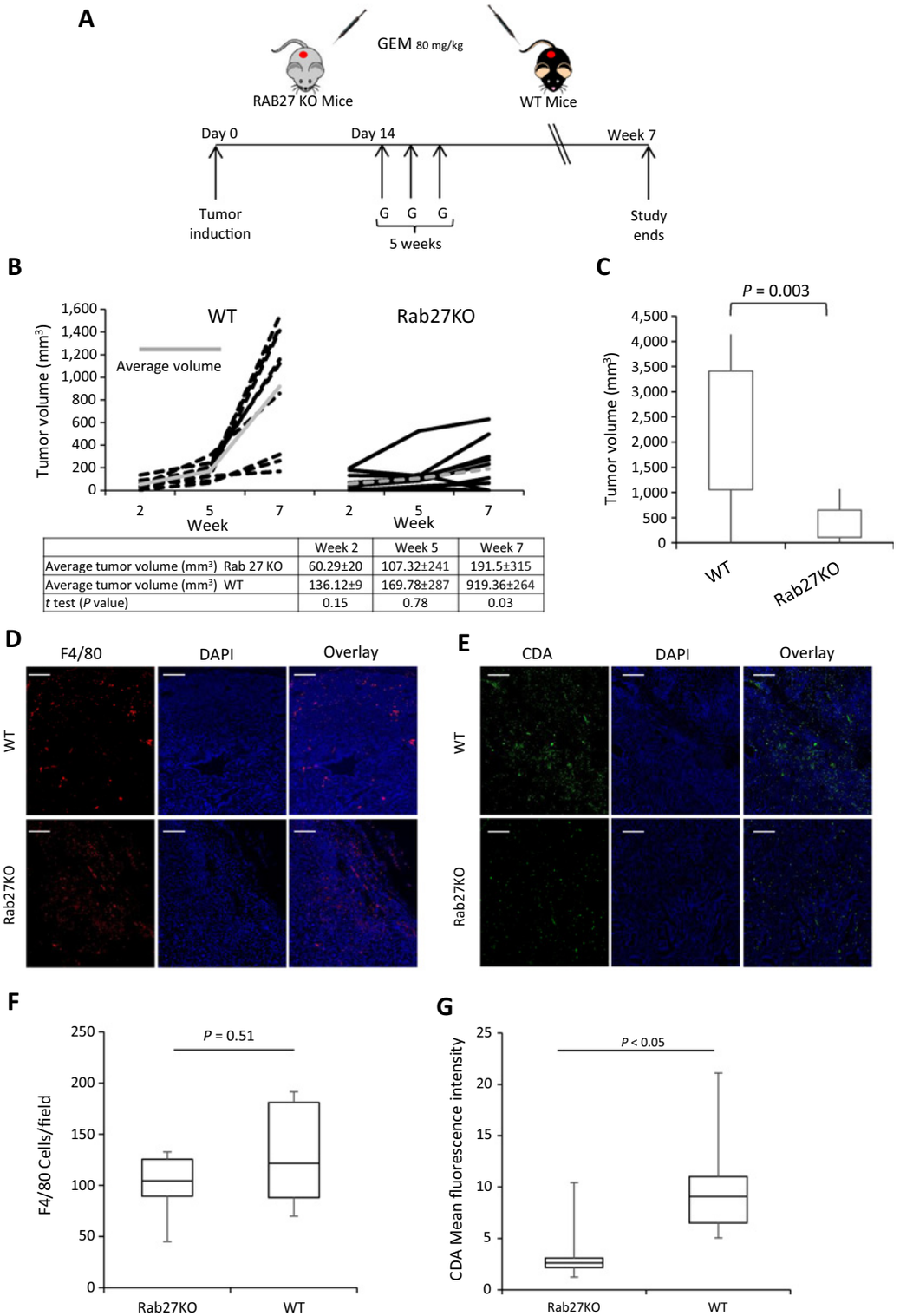

	Week 2	Week 5	Week 7
Average tumor volume (mm³) Rab 27 KO	60.29±20	107.32±241	191.5±315
Average tumor volume (mm³) WT	136.12±9	169.78±287	919.36±264
t test (*P* value)	0.15	0.78	0.03

Figure 5.

MDE and gemcitabine resistance *in vivo*. **A,** Experiment layout. Pancreata of mice were implanted with K989 cells. Gemcitabine was administered after 14 days for 5 weeks. **B,** Tumor volumes in WT and Rab27KO mice at weeks 2–7, measured by ultrasound (gray line, average volume). **C,** Tumor volumes in WT and Rab27KO mice, measured at autopsy ($P = 0.003$). **D,** Immunofluorescence of macrophages (F4/80-red) in WT and Rab27KO mice tumors (bar, 500 μm). **E,** Immunofluorescence of CDA in WT tumors and Rab27KO mice tumors (bar, 500 μm). **F,** Quantification of F4/80 cells/field. **G,** Quantification of mean fluorescence intensity of CDA signal in **E**.

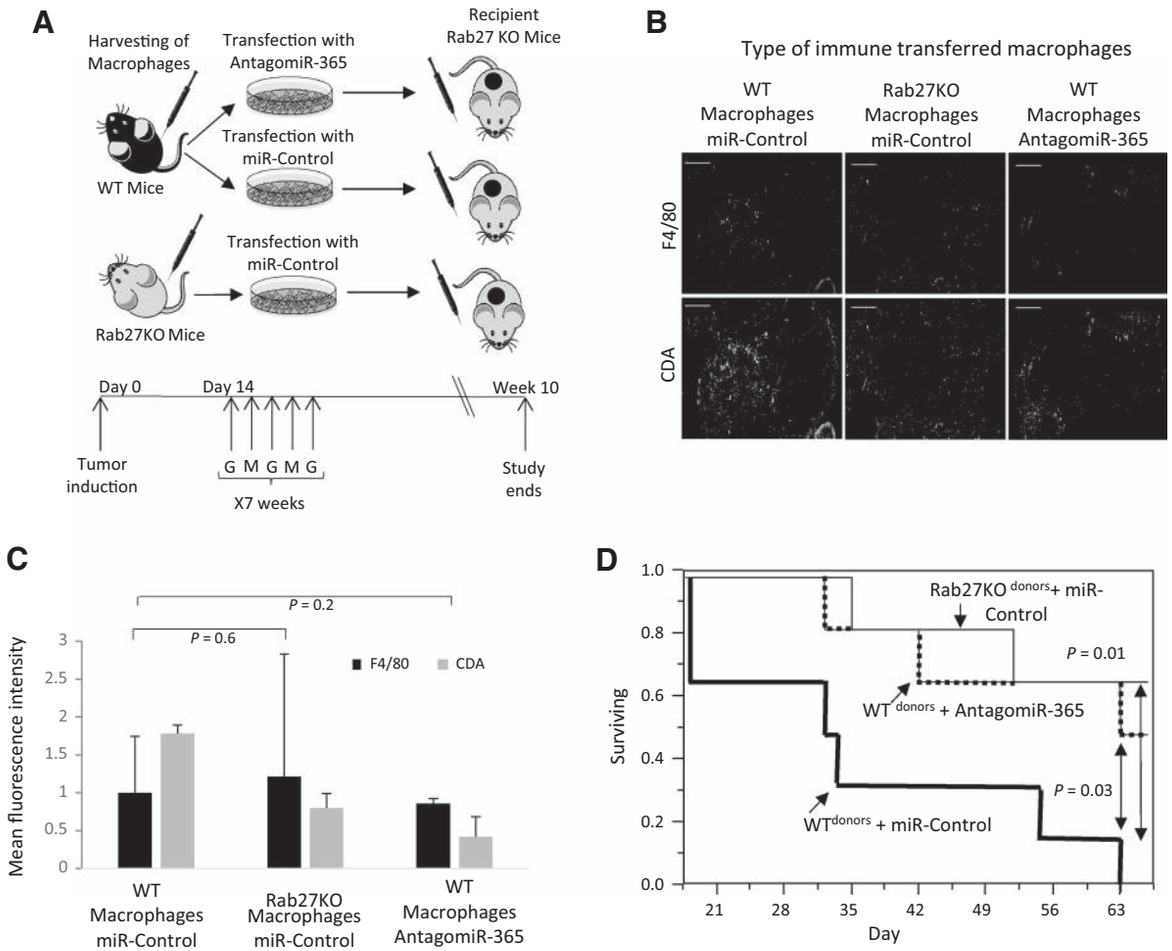

Figure 6.

Immune transfer of mpMacrophages carrying antagomiR-365 *in vivo*. **A,** Two weeks after implantation of K989 tumors in Rab27KO mice, WT and Rab27KO-derived mpMacrophages (transfected with miR-control or antagomiR-365) were injected into the mice. Gemcitabine was administered until week 10. **B,** Immunofluorescence with anti-F4/80 and anti-CDA Abs in PDAC tumors (bar, 500 μm). **C,** Quantification of the pixel area of the CDA and F4/80 signal of the images in **B**. Black bars, F4/80; gray bars, CDA. **D,** Kaplan–Meier graph of the experimental groups in **A**.

inhibit the effect of gemcitabine. However, transfection of antagomiR-365 to K989 cells partially blocked the effect of MDE on gemcitabine ($P = 0.019$). Our observation that antagomiR-365 only partially blocked the effect mediated by MDE raises the possibility that other miRNA delivered by MDE may be involved in the process. Previous works suggested that miR-365 downregulates BCL2, hence hastening apoptosis (37), or participates in signal transduction during mitogenic assault (38). In cutaneous squamous cell carcinoma, miR-365 is considered an oncomiR (39) that acts by targeting nuclear factor I/B (27). Interestingly, miR-193b-mir-365 appears to be involved in metabolic regulation, being essential to brown fat cell differentiation (40), and abundant in the mitochondria (41). Our mass spectroscopy analysis concurred with these data and revealed that miR-365 upregulates pyrimidine metabolism and increases NTP levels in cancer cells. Increased levels of NTP upregulate CDA, one of several deaminases responsible for maintaining the cellular pyrimidine pool (42), and the enzyme responsible for gemcitabine inactivation in humans. CDA expression in PDAC tumors was significantly lower in Rab27KO mice than in WT. Nevertheless, we cannot rule out the possibility that some of the signals we detected in the tumor originate from spillover of CDA from macrophages to cancer cells. CDA deaminates gemcitabine to dFdU (43, 44), which is passively excreted out of the cell. Indeed, we observed increased excretion of dFdU from cancer cells following miR-365 transfection. Alternatively, increased nucleotide pools can affect resistance to gemcitabine by molecular competition (45). Therefore, dCTP upregulated by miR-365 could compete directly with gemcitabine for incorporation into the DNA chain, further potentiating resistance (46, 47). Figure 7 summarizes the proposed mechanism by which macrophages transfer exosomes loaded with miR-365 to PDAC cells and modulate gemcitabine metabolism.

One implication of our study is a possible strategy to overcome gemcitabine resistance by the immune transfer of antagomiR-365 to primary tumors via macrophages. This approach resulted in significant improvement in the effect of gemcitabine on survival of tumor-bearing mice.

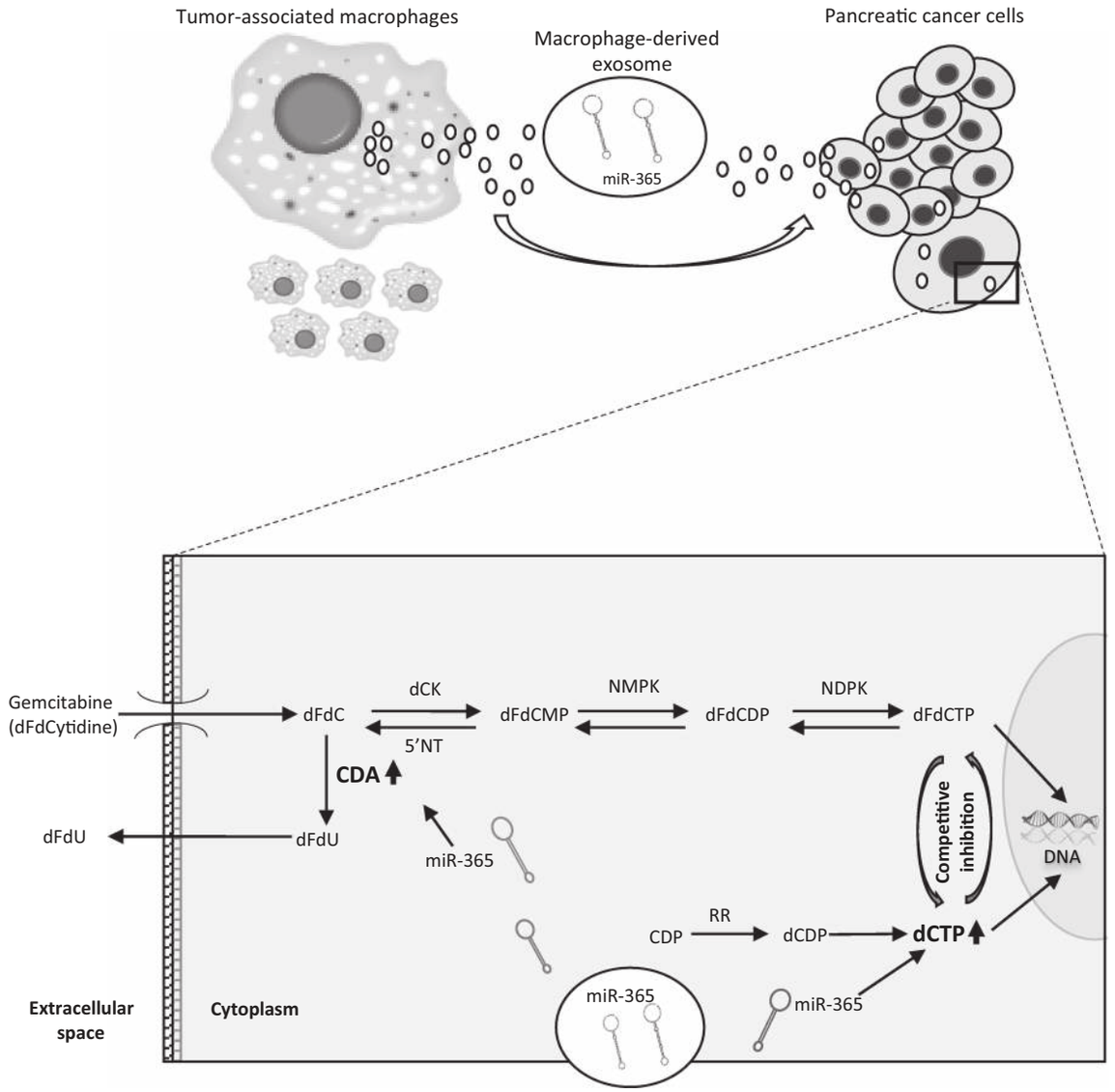

Figure 7.

Summary of the mechanism by which TAM induce gemcitabine resistance. MDE transmit miR-365 selectively to PDAC cells. Gemcitabine (dFdC) is transported into PDAC cells and is phosphorylated by dCK to produce dFdCTP, or deaminated by CDA to dFdU, which is excreted out of the cells. miR-365 is upregulated in PDAC cells and increases the concentration of intracellular NTP, which competes with dFdCTP for DNA incorporation. An increase in NTPs also upregulates CDA expression, further contributing to dFdC deamination. Enzymes and metabolites that regulate gemcitabine resistance are in bold. dCK, deoxycytidine-kinase; CDA, cytidine-deaminase; NMPK, nucleoside monophosphate kinase; NDPK, nucleoside diphosphate kinase; 5′NT, 5′-nucleotidase; RR, ribonucleotide-reductase.

Gemcitabine is the cornerstone of treatment of patients with PDAC, despite its modest efficacy. Our findings suggest a new avenue for the development of interventions aimed to potentiate the effect of gemcitabine. Treatments directed to block the protective effect of macrophages on cancer could prolong survival and reduce morbidity. The knowledge gained from this study is anticipated to be applicable to other cancers for which gemcitabine and other nucleoside analogues are the treatment of choice.

Disclosure of Potential Conflicts of Interest

No potential conflicts of interest were disclosed.

Authors' Contributions

Conception and design: Y. Binenbaum, E. Fridman, Z. Gil

Development of methodology: Y. Binenbaum, Z. Yaari, N. Milman, A. Schroeder

Acquisition of data (provided animals, acquired and managed patients, provided facilities, etc.): Y. Binenbaum, E. Fridman, Z. Yaari, N. Milman, A. Schroeder, G.B. David, T. Shlomi

Analysis and interpretation of data (e.g., statistical analysis, biostatistics, computational analysis): Y. Binenbaum, E. Fridman, N. Milman, A. Schroeder, G.B. David, Z. Gil

Writing, review, and/or revision of the manuscript: Y. Binenbaum, N. Milman, A. Schroeder, Z. Gil

Administrative, technical, or material support (i.e., reporting or organizing data, constructing databases): Y. Binenbaum, G.B. David
Study supervision: N. Milman, T. Shlomi, Z. Gil

Acknowledgments

We thank Lana Ginene and Yotam de la Zerda for technical assistance, Cindy Cohen for her editorial assistance, Naama Koifman and Yeshayahu Talmon and the staff of the imaging unit at the Biomedical Core Facility, and The Ruth and Bruce Rappaport Faculty of Medicine at the Technion for their support. Z. Gil was supported by the Israel Science Foundation. N. Milman was supported by Israel Cancer Research Fund, The Barbara S. Goodman Endowed RCDA for Pancreatic Cancer, and The Israel Cancer Association.

The costs of publication of this article were defrayed in part by the payment of page charges. This article must therefore be hereby marked *advertisement* in accordance with 18 U.S.C. Section 1734 solely to indicate this fact.

Received January 13, 2018; revised May 17, 2018; accepted July 13, 2018; published first July 24, 2018.

References

1. Hidalgo M. Pancreatic cancer. N Engl J Med 2010;362:1605–17.
2. Binenbaum Y, Na'ara S, Gil Z. Gemcitabine resistance in pancreatic ductal adenocarcinoma. Drug Resist Updat 2015;23:55–68.
3. Frese KK, Neesse A, Cook N, Bapiro TE, Lolkema MP, Jodrell DI, et al. Nab-paclitaxel potentiates gemcitabine activity by reducing cytidine deaminase levels in a mouse model of pancreatic cancer. Cancer Discov 2012;2:260–9.
4. Sugimoto M, Mitsunaga S, Yoshikawa K, Kato Y, Gotohda N, Takahashi S, et al. Prognostic impact of M2 macrophages at neural invasion in patients with invasive ductal carcinoma of the pancreas. Eur J Cancer 2014;50: 1900–8.
5. Weizman N, Krelin Y, Shabtay-Orbach A, Amit M, Binenbaum Y, Wong RJ, et al. Macrophages mediate gemcitabine resistance of pancreatic adenocarcinoma by upregulating cytidine deaminase. Oncogene 2014;33: 3812–9.
6. Tolmachova T, Abrink M, Futter CE, Authi KS, Seabra MC. Rab27b regulates number and secretion of platelet dense granules. Proc Natl Acad Sci USA 2007;104:5872–7.
7. Ostrowski M, Carmo NB, Krumeich S, Fanget I, Raposo G, Savina A, et al. Rab27a and Rab27b control different steps of the exosome secretion pathway. Nat Cell Biol 2009;12:19–30.
8. Hingorani SR, Wang L, Multani AS, Combs C, Deramaudt TB, Hruban RH, et al. Trp53R172H and KrasG12D cooperate to promote chromosomal instability and widely metastatic pancreatic ductal adenocarcinoma in mice. Cancer Cell 2005;7:469–83.
9. Kigerl KA, Gensel JC, Ankeny DP, Alexander JK, Donnelly DJ, Popovich PG. Identification of two distinct macrophage subsets with divergent effects causing either neurotoxicity or regeneration in the injured mouse spinal cord. J Neurosci 2009;29:13435–44.
10. Genin M, Clement F, Fattaccioli A, Raes M, Michiels C. M1 and M2 macrophages derived from THP-1 cells differentially modulate the response of cancer cells to etoposide. BMC Cancer 2015;15:577.
11. Théry C, Clayton A, Amigorena S, Raposo G. Isolation and Characterization of Exosomes from Cell Culture Supernatants. Current protocols in cell biology. Hoboken, NJ: John Wiley & Sons, Inc.; 2006. p. 1–29.
12. Réjiba S, Reddy LH, Bigand C, Parmentier C, Couvreur P, Hajri A. Squalenoyl gemcitabine nanomedicine overcomes the low efficacy of gemcitabine therapy in pancreatic cancer. Nanomedicine 2011;7:841–9.
13. Giovannetti E, Del Tacca M, Mey V, Funel N, Nannizzi S, Ricci S, et al. Transcription analysis of human equilibrative nucleoside transporter-1 predicts survival in pancreas cancer patients treated with gemcitabine. Cancer Res 2006;66:3928–35.
14. Bhatnagar S, Shinagawa K, Castellino FJ, Schorey JS. Exosomes released from macrophages infected with intracellular pathogens stimulate a proinflammatory response in vitro and in vivo. Blood 2007;110:3234–44.
15. Ijichi H, Chytil A, Gorska AE, Aakre ME, Bierie B, Tada M, et al. Inhibiting Cxcr2 disrupts tumor-stromal interactions and improves survival in a mouse model of pancreatic ductal adenocarcinoma. J Clin Invest 2011;121:4106–17.
16. Martinez FO, Gordon S, Locati M, Mantovani A. Transcriptional profiling of the human monocyte-to-macrophage differentiation and polarization: new molecules and patterns of gene expression. J Immunol 2006;177: 7303–11.
17. Issman L, Brenner B, Talmon Y, Aharon A. Cryogenic transmission electron microscopy nanostructural study of shed microparticles. PLoS One 2013;8: e83680.
18. Sokolova V, Ludwig A-K, Hornung S, Rotan O, Horn PA, Epple M, et al. Characterisation of exosomes derived from human cells by nanoparticle tracking analysis and scanning electron microscopy. Colloids Surf B Biointerfaces 2011;87:146–50.
19. Van Der Pol E, Hoekstra AG, Sturk A, Otto C, van Leeuwen TG, Nieuwland R. Optical and non-optical methods for detection and characterization of microparticles and exosomes. J Thromb Haemost 2010;8:2596–607.
20. Li J, Liu K, Liu Y, Xu Y, Zhang F, Yang H, et al. Exosomes mediate the cell-to-cell transmission of IFN-α-induced antiviral activity. Nat Immunol 2013; 14:793–803.
21. Azmi AS, Bao B, Sarkar FH. Exosomes in cancer development, metastasis, and drug resistance: a comprehensive review. Cancer Metastasis Rev 2013; 32:623–42.
22. Huang X, Yuan T, Tschannen M, Sun Z, Jacob H, Du M, et al. Characterization of human plasma-derived exosomal RNAs by deep sequencing. BMC Genomics 2013;14:319.
23. Zhao L, Liu W, Xiao J, Cao B. The role of exosomes and "exosomal shuttle microRNA" in tumorigenesis and drug resistance. Cancer Lett 2015;356: 339–46.
24. Hamada S, Masamune A, Miura S, Satoh K, Shimosegawa T. MiR-365 induces gemcitabine resistance in pancreatic cancer cells by targeting the adaptor protein SHC1 and pro-apoptotic regulator BAX. Cell Signal 2013;26:179–85.
25. Ali S, Ahmad A, Banerjee S, Padhye S, Dominiak K, Schaffert JM, et al. Gemcitabine sensitivity can be induced in pancreatic cancer cells through modulation of miR-200 and miR-21 expression by curcumin or its analogue CDF. Cancer Res 2010;70:3606–17.
26. Park J-K, Lee EJ, Esau C, Schmittgen TD. Antisense inhibition of microRNA-21 or -221 arrests cell cycle, induces apoptosis, and sensitizes the effects of gemcitabine in pancreatic adenocarcinoma. Pancreas 2009;38:e190–9.
27. Zhou M, Zhou L, Zheng L, Guo L, Wang Y, Liu H, et al. miR-365 promotes cutaneous squamous cell carcinoma (CSCC) through targeting nuclear factor I/B (NFIB). PLoS One 2014;9:e100620.
28. Guo S-L, Ye H, Teng Y, Wang YL, Yang G, Li XB, et al. Akt-p53-miR-365-cyclin D1/cdc25A axis contributes to gastric tumorigenesis induced by PTEN deficiency. Nat Commun 2013;4:2544.
29. Demontis S, Terao M, Brivio M, Zanotta S, Bruschi M, Garattini E. Isolation and characterization of the gene coding for human cytidine deaminase. Biochim Biophys Acta 1998;1443:323–33.
30. Bobrie A, Krumeich S, Reyal F, Recchi C, Moita LF, Seabra MC, et al. Rab27a supports exosome-dependent and -independent mechanisms that modify the tumor microenvironment and can promote tumor progression and can promote tumor progression. Cancer Res 2012;72:4920–30.
31. McMillin DW, Negri JM, Mitsiades CS. The role of tumour-stromal interactions in modifying drug response: challenges and opportunities. Nat Rev Drug Discov 2013;12:217–28.
32. Chen SJ, Zhang QB, Zeng LJ, Lian GD, Li JJ, Qian CC, et al. Distribution and clinical significance of tumour-associated macrophages in pancreatic ductal adenocarcinoma : a retrospective analysis in China. Curr Oncol 2015; 22:e11–9.
33. Hu H, Hang J-J, Han T, Zhuo M, Jiao F, Wang LW. The M2 phenotype of tumor-associated macrophages in the stroma confers a poor prognosis in pancreatic cancer. Tumour Biol 2016;37:8657–64.
34. Cavel O, Shomron O, Shabtay A, Vital J, Trejo-Leider L, Weizman N, et al. Endoneurial macrophages induce perineural invasion of pancreatic cancer

cells by secretion of GDNF and activation of RET tyrosine kinase receptor. Cancer Res 2012;72:5733–43.
35. Beatty GL, Chiorean EG, Fishman MP, Saboury B, Teitelbaum UR, Sun W, et al. CD40 agonists alter tumor stroma and show efficacy against pancreatic carcinoma in mice and humans. Science 2011; 331:1612–6.
36. Commisso C, Davidson SM, Soydaner-Azeloglu RG, Parker SJ, Kamphorst JJ, Hackett S, et al. Macropinocytosis of protein is an amino acid supply route in Ras-transformed cells. Nature 2013;497:633–7.
37. Singh R, Saini N. Downregulation of BCL2 by miRNAs augments drug-induced apoptosis–a combined computational and experimental approach. J Cell Sci 2012;125:1568–78.
38. Syed DN, Khan MI, Shabbir M, Mukhtar H. MicroRNAs in skin response to UV radiation. Curr Drugs Targets 2013;14:1128–34.
39. Zhou M, Liu W, Ma S, Cao H, Peng X, Guo L, et al. A novel onco-miR-365 induces cutaneous squamous cell carcinoma. Carcinogenesis 2013;34: 1653–9.
40. Sun L, Xie H, Mori MA, Alexander R, Yuan B, Hattangadi SM, et al. Mir193b–365 is essential for brown fat differentiation. Nat Cell Biol 2011; 13:958–65.
41. Barrey E, Saint-Auret G, Bonnamy B, Damas D, Boyer O, Gidrol X. Pre-microRNA and mature microRNA in human mitochondria. PLoS One 2011;6:e20220.
42. Cacciamani T, Vita A, Cristalli G, Vincenzetti S, Natalini P, Ruggieri S, et al. Purification of human cytidine deaminase: molecular and enzymatic characterization and inhibition by synthetic pyrimidine analogs. Arch Biochem Biophys 1991;290:285–92.
43. Abbruzzese BJL, Grunewald R, Weeks EA, Gravel D, Adams T, Nowak B, et al. A phase I clinical, plasma, and cellular pharmacology study of gemcitabine. J Clin Oncol 2014;9:491–8.
44. Bergman AM, Pinedo HM, Peters GJ. Determinants of resistance to 2′,2′-difluorodeoxycytidine (gemcitabine). Drug Resist Updat 2002;5:19–33.
45. Mulcahy LA, Pink RC, Carter DRF. Routes and mechanisms of extracellular vesicle uptake. J Extracell vesicles 2014;3.
46. Valsecchi ME, Holdbrook T, Leiby BE, Pequignot E, Littman SJ, Yeo CJ, et al. Is there a role for the quantification of RRM1 and ERCC1 expression in pancreatic ductal adenocarcinoma? BMC Cancer 2012;12:104.
47. Akita H, Zheng Z, Takeda Y, Kim C, Kittaka N, Kobayashi S, et al. Significance of RRM1 and ERCC1 expression in resectable pancreatic adenocarcinoma. Oncogene 2009;28:2903–9.